Distribution of Active Protein Kinase C in Smooth Muscle

Gerald A. Meininger,* Edwin D. W. Moore,# David J. Schmidt,§ Lawrence M. Lifshitz,§ and Frederic S. Fay§

*Cardiovascular Research Institute, Department of Medical Physiology, College of Medicine, Texas A&M University Health Science Center, College Station, Texas 77843 USA; #Department of Physiology, University of British Columbia, Vancouver, British Columbia V6T 1Z3, Canada; and §Program in Molecular Medicine and the Biomedical Imaging Group, University of Massachusetts Medical School, Worcester, Massachusetts 01605 USA

ABSTRACT To localize activated protein kinase C (PKC) in smooth muscle cells, an antibody directed to the catalytic site of the enzyme was used to assess PKC distribution by immunofluorescence techniques in gastric smooth muscle cells isolated from *Bufo marinus*. An antibody to vinculin was used to delineate the cell membrane. High-resolution three-dimensional images of immunofluorescence were obtained from a series of images collected through focus with a digital imaging microscope. Cells were untreated or treated with agents that increase PKC activity (10 μM carbachol for 1 min, 1 μM phorbol 12-myristate 13-acetate (PMA) for 10 min), or have no effect on PKC activity (1 μm 4-α phorbol, 12,13-didecanoate (4-α PMA)). In unstimulated cells, activated PKC and vinculin were located and organized at the cell surface. Cell cytosol labeling for activated PKC was sparse and diffuse and was absent for vinculin. After treatment with carbachol, which stimulates contraction and PKC activity, in addition to the membrane localization, the activated PKC exhibited a pronounced cytosolic fibrillar distribution and an increased total fluorescence intensity relative to vinculin. The distributions of activated PKC observed after PMA but not 4-α PMA were similar to those observed with carbachol. Our results indicate that in resting cells there is a pool of activated PKC near the cell membrane, and that after stimulation activated PKC is no longer membrane-confined, but is present throughout the cytosol. Active PKC appears to associate with contractile filaments, supporting a possible role in modulation of contraction.

INTRODUCTION

Protein kinase C (PKC) is a central component in the transduction pathway linked to phospholipid turnover in the plasma membrane (Andrea and Walsh, 1992; Asuoka et al., 1993; Haller et al., 1990; Langlands and Diamond, 1992; Nishizuka, 1984). In smooth muscle PKC is considered to play a significant role in mediating agonist-stimulated short-term cellular responses associated with contraction and changes in ionic distribution, as well as longer-term cellular events such as cell growth, differentiation, and hypertrophy (Andrea and Walsh, 1992; Asuoka et al., 1993; Nishizuka, 1984). Phosphorylation of specific target proteins by PKC determines the pathways that are regulated by this kinase. Those targets are, in turn, determined not only by substrate specificity of this enzyme family, but also by substrate accessibility to PKC, since its distribution is altered after activation.

Cell fractionation methods provided some of the earliest information regarding changes in the distribution of PKC, revealing that stimuli that caused its activation appeared to induce a shift in it's distribution from a soluble "cytosolic" fraction to a particulate, "membrane" fraction (Haller et al., 1990; Langlands and Diamond, 1992). While these results provided an easy explanation for why stimuli that activate PKC also trigger phosphorylation of membrane proteins and cause changes in numerous membrane-associated functions in intact cells, they provided little aid in understanding why these same stimuli also trigger phosphorylation of numerous cytoskeletal/contractile proteins.

Investigators using standard, nonquantitative immunofluorescence and imaging methods in intact cells have increasingly reported PKC localizations to other subcellular structures such as focal contacts, cytoskeleton, and nuclei (e.g., Haller et al., 1994; Khalil et al., 1992; Khalil and Morgan, 1991; Liu et al., 1989; Mochly-Rosen, 1995; Mochly-Rosen et al., 1990). Evidence has also accumulated to indicate the existence of multiple isoforms of PKC that are classified in subfamilies of similar genetic origin, structure, and regulation (Andrea and Walsh, 1992; Asuoka et al., 1993; Hug and Sarre, 1993; Morgan and Morgan, 1984). In addition, it is clear that multiple isoforms of PKC are often co-expressed in any given cell and that the various isoforms can regulate different cellular processes (Haller et al., 1994; Khalil and Morgan, 1992; Liu et al., 1989; Morgan and Morgan, 1984). There is, therefore, increased interest in precisely establishing the subcellular localization and possible translocation for each of the PKCs associated with specific cellular responses.

Studies utilizing fluorescent phorbol esters as well as antibodies to PKC and its various isotypes have been utilized in smooth muscle cells (Ali et al., 1994; Andrea and Walsh, 1992; Assender et al., 1994; Donnelly et al., 1995; Haller et al., 1994; Khalil et al., 1992; Khalil and Morgan, 1991, 1992; Schwartz, 1992). They have shown increased staining of the surface membrane, perinuclear regions, and nucleus that occurs within minutes following stimulation of

Received for publication 30 March 1998 and in final form 28 April 1999.

Address reprint requests to Gerald A. Meininger, Ph.D., Department of Medical Physiology, College of Medicine, Texas A&M University Health Science Center, College Station, TX 77843-1114. Tel.: 409-845-7491; Fax: 409-847-8635; E-mail: gam@tamu.edu.

This paper is dedicated to the memory of Fred Fay.

0006-3495/99/08/973/12 $2.00

cells with agonists expected to increase PKC activity (Andrea and Walsh, 1992; Haller et al., 1994; Khalil et al., 1992; Khalil and Morgan, 1991, 1992). The temporal relationships between these translocation events and the changes in smooth muscle function that ensue after PKC activation have not been completely resolved. For example, it is noteworthy that many of the translocation events that occur are complete within minutes. However, the contraction that occurs after PKC activation is typically slowly developing and generally begins within 10 min but does not reach a sustained maximum for 30 to 60 min (Andrea and Walsh, 1992; Walsh et al., 1993). As one approach to understanding the redistribution of PKC after activation, we carried out studies first to further characterize an antibody that preferentially binds to activated PKCs, and then to utilize immunofluorescent labeling in conjunction with high-resolution three-dimensional (3D) microscopic imaging to analyze the distribution of activated PKC in single isolated smooth muscle cells both at rest and after stimulation with agonists expected to increase PKC activity.

METHODS

Specificity of the anti-PKC and preferential binding to active PKC

A monoclonal anti-PKC antibody developed by Mochly-Rosen and Koshland (1987, 1988) was chosen for these studies as prior observations suggested that it might recognize an epitope on different PKCs that is expressed only upon activation of PKC. In this previous work, Mochly-Rosen and Koshland (1988) used a PKC activity assay to detect and identify inhibitory antibodies that specifically inhibited activity of intact, nondenatured, highly purified, rat brain PKCs. The properties of several such antibodies were further investigated (Mochly-Rosen and Koshland, 1987, 1988), including the IgM designated MAb 1.9, which reportedly displayed unique behavior in several assays. First, the MAb 1.9 directly inhibited the activity of purified intact mixed PKC isoforms. Second, they found that it also inhibited the unregulated constitutively active catalytic domains of mixed PKC isoforms created by partial trypsin proteolysis. In contrast, it had no effect (Mochly-Rosen and Koshland, 1987) on the activity of the closely related cAMP-dependent protein kinase (Hanks and Hunter, 1995; Nishizuka, 1992), indicating specificity for the PKC catalytic domain. Third, they reported that the epitope recognized by MAb 1.9 also appears to be functionally linked to the catalytic domain, since ATP binding to PKC diminished binding of MAb 1.9. Finally, a dependence of MAb 1.9 binding to PKC when the enzyme is in an activated and/or semi-denatured state was suggested by its complete lack of binding in SDS-Page, but the retention of binding in immunofluorescence, immunoprecipitation, and ELISA. Based on these findings, we reasoned that the activated state would expose the catalytic epitope for MAb 1.9. We therefore also performed several experiments to address this issue and further test the properties of MAb 1.9 under conditions that activate PKCs in vitro and in vivo.

PKCs from either rat brain protein extract or toad stomach protein extract were immunoprecipitated with MAb 1.9. The immunoprecipitation procedure was required because the anti-PKC IgM, MAb 1.9, is not useful for Western blotting, as was previously reported (Mochly-Rosen and Koshland, 1987). These experiments allowed us to determine whether MAb 1.9 preferentially recognized activated PKC. This was accomplished by mixing MAb 1.9 with varying concentrations of phorbol 12-myristate 13-acetate (PMA) (10^{-9}-10^{-6} M), and phosphatidylserine (1 mg/ml) with protein extracts containing PKC. To this mixture was added an anti-IgM bound to Protein A Sepharose. After 1-h incubation followed by centrifugation, the supernatant was removed and the Sepharose pellet rinsed with a 20 mM Tris buffer. The rinsed pellet was then mixed with sample buffer and boiled to free PKC from the antibodies. Identical volumes of sample buffer were loaded on an SDS-PAGE gradient gel (9.5–16%). The gel was blotted onto nitrocellulose (Western blot) and reacted with a rabbit polyclonal anti-pan-PKC (2 μg/ml; Upstate Biotechnology Inc., 06-155) followed by an HRP-labeled goat anti-rabbit IgG secondary (Jackson ImmunoResearch). Labeled PKC was detected with an ECL chemiluminescent system (Amersham Corporation). Bands on the developed film were quantitated on a Visage System (Kodak) and expressed as integrated optical density.

In a second set of experiments, fresh tissue slices (~200 μM thick) were made from toad stomach after removal of the mucosa. These tissue slices were incubated in either amphibian Kreb's Ringer (AKR) alone, AKR containing 10 μM carbachol for 1 min, AKR with 1 μM PMA for 10 min, or AKR with 1 μM 4-α PMA for 10 min. Tissue slices were fixed with paraformaldehyde and permeabilized with Triton X-100. Tissue selections were cut into 1-mm^2 sections, placed in 2 M sucrose on a mounting peg, and frozen in liquid N_2. Frozen pieces were cryosectioned (Reichert Ultra Cut, FC4E) into 8–10-μM-thick sections and were placed on a glass slide and immunofluorescently labeled for PKC and vinculin as described above. Images of sections were obtained using a confocal microscope (Biorad MRC 600). Images were background-subtracted and total integrated optical density was measured in a 100 $\times$ 100 pixel square. Fluorescence was expressed as a ratio of PKC/vinculin fluorescence.

In a final set of experiments, colocalization of MAb 1.9 with a polyclonal pan-PKC antibody (Santa Cruz Biotechnology Inc., sc-77) was assessed in PMA-stimulated tissue. In these studies, freshly isolated toad stomachs were cut in cross-sections, equilibrated in oxygenated AKR, exposed to 100 nM PMA in AKR for 30 s, then blotted and flash-frozen in liquid N_2-cooled isopentane. Cryosections (10 μM) were then cut from frozen cross-sectional pieces with a cryostat, and thawed in the presence of 4% paraformaldehyde in PBS at 4°C. Fixation was allowed to proceed for 10 min with warming to room temperature. Sections were then permeabilized and immunolabeled as described above for cells, with the following exceptions. First, sections were placed in blocking buffer (3% goat serum, 2% BSA, 0.05% Triton X-100, and 0.02% NaN_3 in PBS, pH 7.4) in a humidified chamber for 1 h to minimize nonspecific antibody binding. Second, primary antibodies (MAb 1.9 at 50 μg/ml, polyclonal pan-PKC at 1:100 dilution) were applied simultaneously in this blocking buffer. Third, whole secondary antibodies were used, and included goat anti-mouse IgM-μ (rhodamine-labeled, 1:100) and goat anti-rabbit IgG (H+L, serum-absorbed, fluorescein-labeled, 1:100). And finally, repeated final washes with PBS were followed by mounting in 2% DABCO mounting media mixed with 190-nM diameter broad-spectrum fluorescent latex beads for use in image alignment.

Cell preparation and labeling

Smooth muscle cells were enzymatically isolated from the stomach of the toad *Bufo marinus* as previously described (Fay et al., 1982). Isolated cells were suspended in an amphibian physiological saline solution (AKR) containing (in mM): NaCl (108.9), KCl (3.0), $NaH_2PO_4 \cdot H_2O$ (2.2), $MgSO_4$ (0.97), $Na_2HPO_4 \cdot 7H_2O$ (0.55), $NaHCO_3$ (200), and $CaCl_2$ (1.8). For immunocytochemistry, cells were allowed to settle for 60–90 min onto poly-L-lysine-coated glass coverslips (0.5%) that had been acid and ethanol washed. Before fixation, cells were exposed to either 10 μM carbachol for 1 min, 1 μM phorbol 12-myristate 13-acetate (PMA) for 10 min, or 1 μM 4-α phorbol 12,13-didecanoate (4-α PMA, an inactive phorbol conjugate) for 10 min, or were exposed only to AKR. Cells were then fixed by immersion in 2% paraformaldehyde in phosphate-buffered saline (PBS) for 10 min (pH 7.4) containing (in mM): KCl (2.7), KH_2PO_4 (1.5), NaCl (137), and Na_2HPO_4 (8.0), followed by washes in glycine buffer (0.1 M, pH 7.4) to quench unreacted aldehyde. Fixed cells were permeabilized with 0.1% Triton X-100 for 10 min followed by washes in PBS.

After rinsing, cells were labeled simultaneously with two primary antibodies. Primary antibodies were 1) a mouse monoclonal IgG raised

against chicken gizzard vinculin (100 μg/ml; Sigma, VIN 11–5), which we have previously reported recognized primarily a single band at 135 kDa in unboiled toad stomach extracts on Western blots (unpublished observation), and 2) a mouse monoclonal IgM prepared against a highly purified mixture of rat brain PKCs containing both particulate-extracted (active) and cytosolic PKCs (Mochly-Rosen and Koshland, 1987, 1988), (40 μM/ml; GIBCO-BRL, MAb 1.9). Primary and secondary antibodies were dissolved in a sodium citrate buffer containing (in mM): NaCl (300), Na_3 citrate (30), 2% goat serum, 1% bovine serum albumin (BSA), 0.05% Triton X-100, and 0.02% NaN_3. All antibody incubations were from 60 min. Excess unbound antibody was removed with washes in PBS containing 0.1% Triton X-100.

Secondary antibody for anti-PKC was a goat anti-mouse IgM heavy chain (μ) specific Fab fragment that was labeled with fluorescein (Jackson ImmunoResearch). Secondary antibody for anti-vinculin was a goat anti-mouse IgG heavy chain (γ) specific Fab fragment that was labeled with Texas Red. Coverslips with labeled cells were mounted on glass slides with 9:1 glycerol/10× PBS and DABCO (1% w/v) mounting medium. In addition, 190-nm beads with a broad fluorescent emission (510–665 nm; Molecular Probes) where fluorescence could be recorded by both fluorescein and Texas Red Filter sets were mixed with the mounting medium to act as fiduciary markers for alignment of images. To assess nonspecific binding of secondary antibodies from specific binding to primary antibodies, cells were labeled without permeabilization, or with each secondary antibody alone. Autofluorescence was assessed in unlabeled cells. Also, some cells were labeled with a nonspecific mouse IgM as the primary antibody.

3D microscopy

Images of labeled cells were acquired with a Zeiss IM-35 microscope equipped with a 100 W mercury arc lamp for epifluorescence microscopy. Cells were viewed with a 60× Nikon (NA 1.4) planapo objective and 16× eyepiece, and images were captured by a Photometrics thermoelectrically cooled CCD camera (RCA 501 chip). A PC was used to control a stepper motor attached to the fine focus and the position of the objective relative to the stage was monitored with an eddy-current sensor. Additionally, a controlled shutter regulated the duration of illumination (Fay et al., 1989). Digitized images of labeled cells were obtained at 0.25 μm intervals. This through-focus image series was transferred to Silicon Graphics workstations for analysis. In addition, a through-focus set of images was acquired of fluorescent beads 190 nm in diameter. The beads were labeled with fluorescein, rhodamine, and Texas Red and provided an empirical measure of the microscope point spread function under optical conditions identical to those in which images from labeled cells were acquired.

Image restoration and analysis

To prepare images for analysis, the dark-current and background were subtracted from and the result was then flat-field corrected for nonuniformities in illumination intensity and camera sensitivity across the field of view. Three-dimensional data sets were processed using a constrained deconvolution algorithm based on regularization theory (Carrington, 1990; Carrington et al., 1990; Fay et al., 1989) to reverse blurring introduced by microscope optics. Image pairs were aligned using the fiduciary markers, and to eliminate nonspecific signal, restored images were thresholded using an intensity value that eliminated 99% of the signal detected in restored images of cells labeled with secondary antibody alone.

To find the surface of the cells we defined a function that corresponded to a cylinder that was positioned around the outside of the cell, but not touching it. The outline of the cylinder was allowed to deform to points of maximum fluorescent intensity on the cell surface (Moore et al., 1993; Lifshitz, 1998). Cell surface coordinates obtained in this fashion were used to define a cell boundary zone that was 0.45 μm on either side of the identified cell edge. To further improve identification of point sources of fluorescence, data within the boundary annulus were convolved with the image of a restored 190-nm fluorescent bead (analogous to using a matched filter). Points in the convolved image that were local maxima in z (i.e., vertical optical axis) were identified as the true position of structures which remained partially blurred after restoration due to poorer resolution along the vertical axis of the microscope. The resulting one-voxel annulus (150 nm^3/voxel) was defined as the vinculin-localized cell surface (Moore et al., 1993; Lifshitz, 1998).

Fig. 1 illustrates the processes of image restoration, segmentation, and

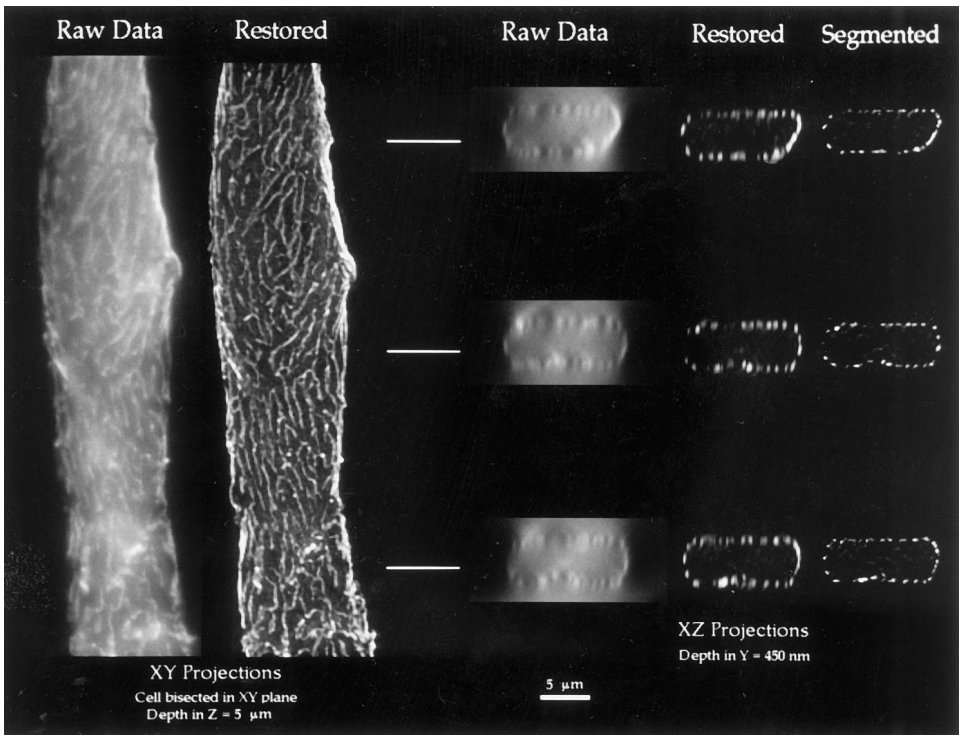

FIGURE 1 Demonstration of image restoration, segmentation, and cell surface localization. A fixed cell is shown labeled with anti-vinculin IgG and an anti-mouse secondary antibody conjugated to Texas Red. The data set for this cell contained 42 2D image planes, of which 20 are displayed before and after restoration in the bisected cell image on the left. Images on the right were obtained by rotating the 3D cell image by 90° about the y axis and segmenting the data set to display 450-nm-thick sections along the x-z axes. To improve the definition of the surface of cells from anti-vinculin images, the image of the cell was convolved with the image of a restored fluorescent bead to identify fluorescent points of maximum intensity.

cell surface localization used to analyze the distribution of PKC and vinculin at near-membrane sites. The cell depicted in this figure was labeled with an anti-vinculin IgG and an anti-mouse Fab fragment conjugated with rhodamine. The full data set for this cell contained 42 image planes acquired at 0.25-μm intervals. To avoid superimposition of front and back surfaces, the cell is shown bisected in the *x, y* plane, and 20 planes of data in *z* are displayed before and after restoration. Cross-sections, 0.45 μm thick, are also displayed before and after restoration. Approximately 90% of total vinculin fluorescence was located at the cell surface within a 150-nm-wide annulus.

Fluorescein anti-PKC signal was considered to colocalize with Texas Red anti-vinculin signal if it had the same *x* and *y* coordinates and had a *z* coordinate that was no more than 1 voxel (150 nm) away from the maxima. Colocalization was constrained so that only one voxel with signal specific for PKC could colocalize with only one voxel with signal specific for vinculin. Criteria for colocalization in *z* were relaxed as previously described by this laboratory, to allow for more limited resolution along the *z* axis and corresponding uncertainty in defining the true *z* position (Moore et al., 1993; Lifshitz, 1998). Cell boundary coordinates were used to define the distribution of PKC-specific fluorescence as a function of distance from the cell membrane and fluorescent intensity per voxel.

RESULTS

Anti-PKC specificity and preferential binding to active PKC

Experiments were carried out to determine whether MAb 1.9 preferentially identified activated PKC over the nonactivated kinase. Figs. 2 and 3 show the results of an experiment to determine whether the binding of MAb 1.9 to PKC is enhanced by its activation, as would be expected if epitope exposure is activation-dependent. Specifically, protein kinase C in protein extracts from both rat brain (Fig. 2) and toad stomach (Fig. 3) were activated by increasing levels of PMA (10^{-9}-10^{-6} M) and the ability of MAb 1.9 to immunoprecipitate PKC was determined. Immunoprecipitated PKC was run on a Western blot and identified and quantified using a polyclonal anti-pan-PKC, which primarily detected a band at ~97 kDa. We found that MAb 1.9-mediated immunoprecipitation of PKC was increased in a dose-dependent fashion by PMA pretreatment of the reaction mixture for both rat brain protein extract (Fig. 2) and toad stomach protein extract (Fig. 3). The effect of PMA was specific for the predominant 97-kDa band identified as PKC with the polyclonal antibody. Toad stomach PKC was therefore clearly recognized by this antibody, and this recognition dramatically increased with application of very low doses of PMA, which are known to activate PKC. While the extent of binding of PKC to MAb 1.9 increased after exposure of tissue to PMA in extracts from both rat brain and toad stomach, the shape of the concentration-response relationships differed between the rat brain and toad stomach. The precise reason for this difference is unclear. It may well reflect differences between these preparations in the extent of proteolysis, the presence of endogenous activators, or presence of different PKC isoforms between rat and toad, leading to differences in the fraction of PKC molecules that are active in the absence of PMA. It is clear, however, that the extent of binding was enhanced in the presence of 1 μM PMA, which was the concentration of PMA utilized for the immunolabeling experiments.

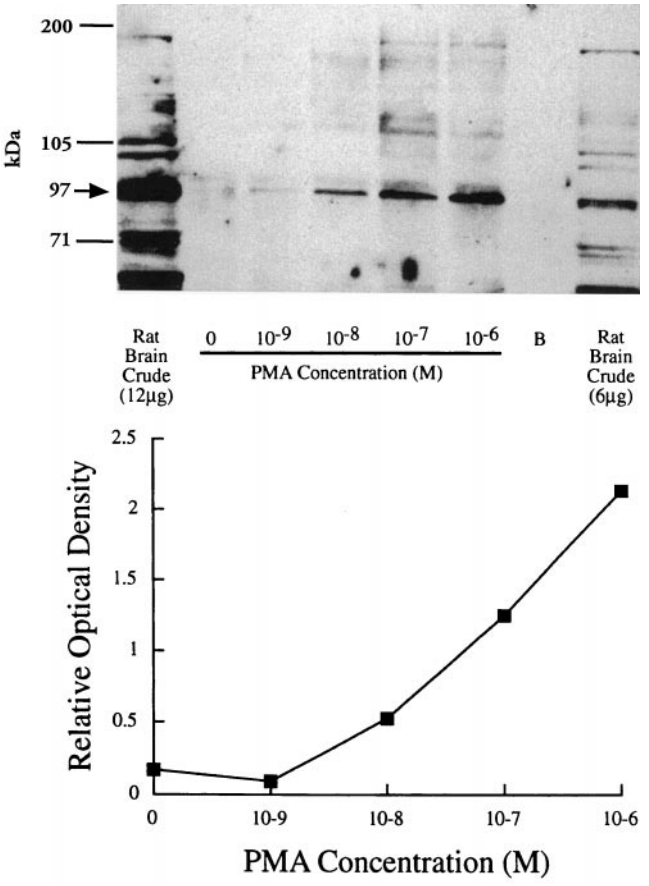

FIGURE 2 Demonstration of immunoselectivity of anti-PKC IgM (MAb 1.9) for the active form of PKC in rat brain cell lysate. *Top:* Immunoprecipitation of PKC from rat brain with the MAb 1.9. First and last lanes show rat brain protein extract run for comparison without immunoprecipitation. From left to right, lanes 2–6 show amount of immunoprecipitated PKC after addition of increasing concentrations of PMA. Lane 7 was a buffer-only blank (B). *Bottom:* Optical density measurements of the blot. Relative optical density of the bands corresponding to PKC in lanes 2–6 are plotted versus the PMA concentration. Effects of PMA on band density were consistently confined to the band identified as PKC.

To examine whether anti-PKC IgM had retained its specificity for the activated form of PKCs after fixation under conditions required for the immunolocalizing experiments, we studied the effect of activation on immunolabeling efficiency in toad stomach. This was accomplished using fresh tissue slices of toad stomach (~200 μm thick) that were then incubated with AKR alone or with added PMA, 4-α PMA, or carbachol. These thin slices were then fixed and immunofluorescently labeled for PKC and vinculin, and measurements of total PKC-specific and vinculin-specific fluorescence obtained from confocal images. A ratio of PKC/vinculin fluorescence is presented in Fig. 3. We found that after treatment with PMA and carbachol, but not 4-α PMA, the fluorescence ratio was significantly increased by 150% and 227%, respectively (Fig. 3), demonstrating enhanced binding of the anti-PKC antibody. The ratio of PKC

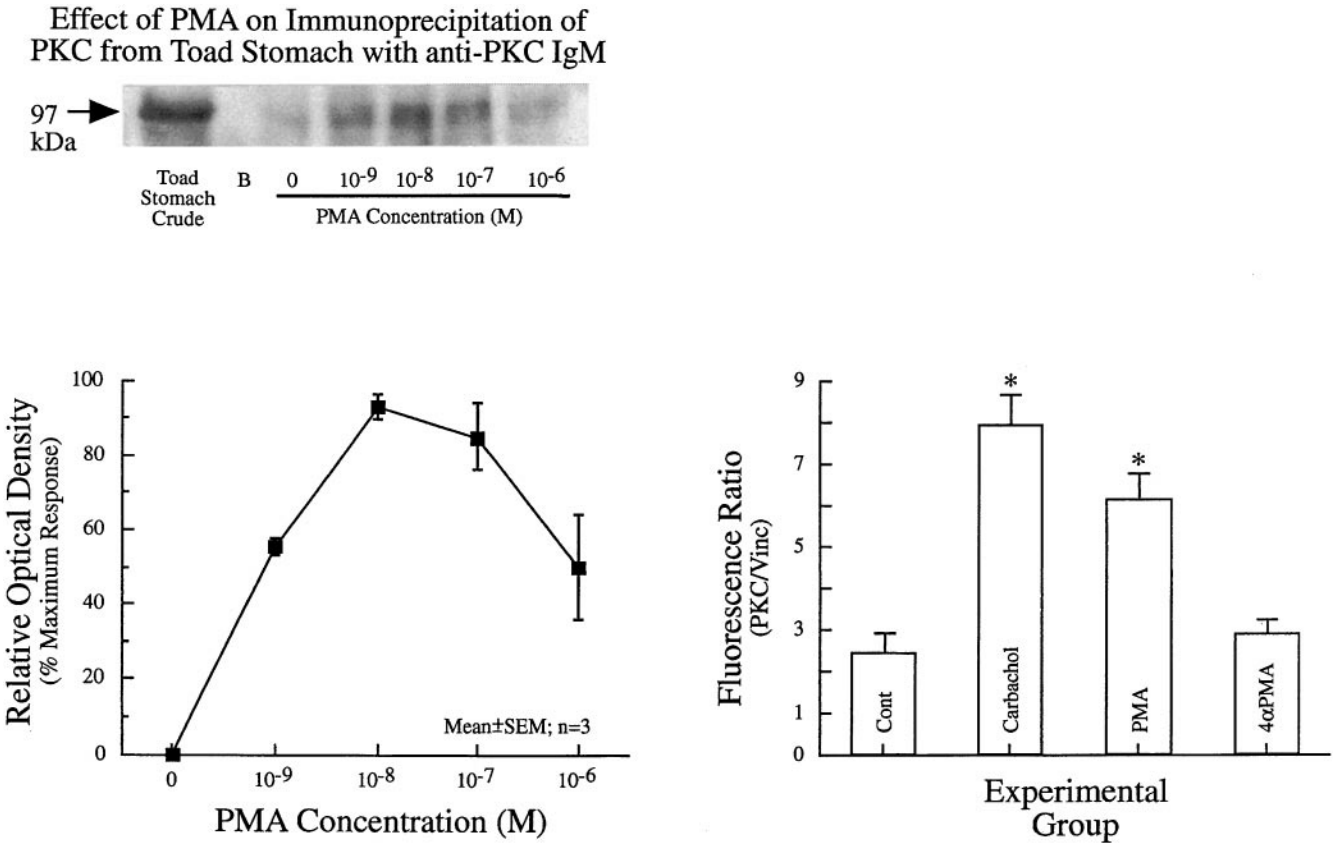

FIGURE 3 Demonstrations of immunoselectivity of anti-PKC IgM (MAb 1.9) for the active form of PKC toad stomach cell lysate. *Top left:* Immunoprecipitation of PKC from toad stomach with MAb 1.9 IgM used for immunofluorescent localization of PKC. The first lane shows toad stomach protein extract run for comparison, without immunoprecipitation. The second lane was a buffer-only blank (B). From left to right, lanes 3–7 show amount of immunoprecipitated PKC after addition of increasing concentrations of PMA. The band position corresponding to the reported molecular weight for PKC is ~97 kDa. *Bottom left:* Optical density measurements of the blot shown at top left. Relative optical density of bands corresponding to PKC in lanes 3–7 are plotted versus concentration of PMA in the immunoprecipitation reaction mixture. Dose-dependent changes in optical density were confined to the band identified as PKC. *Bottom right:* Quantitation of binding of MAb 1.9 to thin slices of toad stomach tissue after stimulation with carbachol (10 μm for 1 min) or PMA (1 μm for 10 min). Average fluorescence intensity per pixel with MAb 1.9 was normalized with anti-vinculin labeling in the same field to correct for differences in amount of tissue between sections.

to vinculin fluorescence corrects for variability in the number of cells in a given microscopic field and nonspecific variations in labeling efficiency. These results indicate that the anti-PKC IgM MAb 1.9 epitope was preserved in fixed tissue and again demonstrated activation-dependent accessibility.

Finally, to directly test whether MAb 1.9 was PKC-specific in this tissue, we compared MAb 1.9 colocalization with a pan-PKC antibody after PMA stimulation. As shown in Fig. 4, a highly significant (nonrandom) colocalization for dual labeling with MAb 1.9 and pan-PKC antibody was found. MAb 1.9 colocalization with anti-pan-PKC averaged 55.9 ± 13.9% (mean ± SD), a level of colocalization very close to that observed when two antibodies are used to recognize the same epitope in this tissue. The fact that the maximum level of colocalization that can be achieved is <100% reflects 1) small residual errors in registration of image pairs where these pairs are aligned to the nearest pixel (Moore et al., 1993); and 2) an area of a small but finite probability that the antibody fails to find or stay bound to its epitope (Mochly-Rosen and Koshland, 1988).

Distribution of activated PKC in smooth muscle: restored images

Restored images of a cell at rest and a carbachol-treated cell labeled for activated PKC and vinculin are shown in Fig. 5. From restored images of the resting cell, it can be seen that active PKC (*left-hand panels*) is distributed in an annular manner near the cell membrane defined by the distribution of vinculin (*right-hand panels*). Specific labeling is apparent in top and bottom surface views, but is noticeably absent in sections through the cell center. Active PKC, like vinculin, is not diffusely distributed but appears organized as strands which are oriented along the cell's long axis and are nearly parallel. The bands are spaced ~0.5 μm apart. No specific labeling was detected in nonpermeabilized cells or cells treated with the secondary antibody alone.

After treatment of cells with carbachol (*bottom panels*), the distribution of active PKC was significantly changed so that activated PKC-specific label was now clearly apparent throughout the interior of the cell. The pattern of distribution within the cytosolic region was very filamentous and

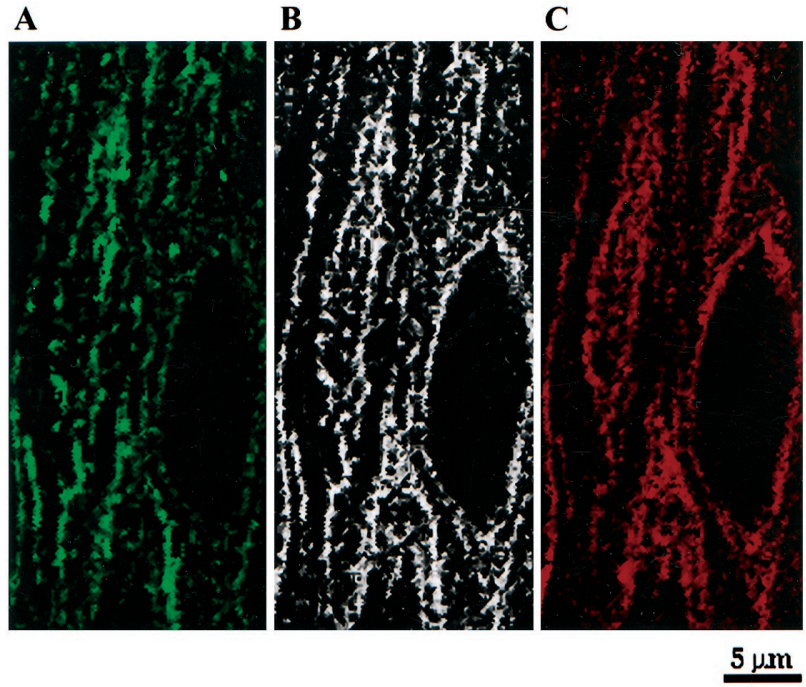

FIGURE 4 MAb 1.9 and pan-PKC antibodies label the same structures in toad gastric smooth muscle after 100 nM PMA stimulation (30 s). The end panels above depict the distribution of MAb 1.9 (*A*) and Santa Cruz polyclonal pan-PKC (*C*) in the smooth muscle layer of a 10 μm section of PMA-stimulated, flash-frozen toad stomach (60× objective, 5× eyepiece). The images shown are opaque 3D projections of fluorescence intensity in a 1-μm-thick subsection (four *z* planes) of smooth muscle after image restoration, image alignment with fiduciary marker beads, and detection of *z* axis maxima as described in the text. Processing of these images included quantification of nonspecific fluorescence in noncellular regions and background subtraction to remove 99% of this fluorescence. The center panel (*B*) depicts the two datasets projected together, with colocalizing voxels shown in white and no relaxation of *z* axis colocalization requirements as for cell analysis. Calculation of colocalization statistics for 62 1-μm^3 areas randomly chosen from muscle cell areas indicates that the probability of this degree of colocalization being due to chance is $p = 0.000058$ (versus random and independent placement of the same number of voxels found in the two images).

remarkably similar to previously reported distribution patterns observed for calponin, actin, and tropomyosin (Walsh et al., 1993). There was no visible activated PKC labeling in the nuclear region. Carbachol had no evident effect on the distribution pattern of vinculin. Treatment of smooth muscle cells with PMA, but not 4-α PMA (Fig. 6), produced a change in distribution that was similar to that seen with carbachol. Activated PKC was visibly organized in filament-like strands through the cytosol but not in the nuclear region. Vinculin distribution was also unaffected by PMA.

In Fig. 7, the cells were rotated 90° about their *x* axis to display cross-sections. Each cross-section displayed is 150 nm thick and represents a cross-sectional view taken from the cell region indicated by arrows in the margins of Figs. 5 and 6. Cross-sectional images have been pseudocolored to display PKC as green and vinculin as red, and images have been superimposed. If voxels are green they contain only activated PKC, if they are red they contain only vinculin, if they are white they contain both vinculin and activated PKC, and if they are black they contain neither protein. Cross-sectional views clearly show the increase in activated PKC within the cytosol. To facilitate visualization of changes in activated PKC distribution in a larger portion of the smooth muscle cell, a control cell and a carbachol-treated cell are shown as stereo image pairs in Fig. 8. Stereo pairs clearly illustrate the annular distribution of vinculin in red overlying a subsurface pool of activated PKC in green. Furthermore, the distribution of the activated PKC appears to mirror the distribution of the vinculin, but to be offset from it toward the interior of the cell. The increase in activated PKC labeling within the cell center is readily apparent in the carbachol-treated cell.

Quantitative analysis of 3D fluorescence images

The distribution of activated PKC in resting toad stomach smooth muscle cells was subjected to extensive analysis in reference to the vinculin label, a marker for the cell membrane. Quantitative analysis of overlap between activated PKC and vinculin indicated that in the unstimulated cell 40.8% of activated PKC-specific signal was within the 150 nm annular region defined by vinculin label. Of this annular activated PKC, 17.9% of the voxels containing activated PKC also contained vinculin. These vinculin-containing voxels represented only 10.8% of total vinculin (Table 1). Colocalization of these two proteins was significantly less than could be accounted for by chance alone. Remaining activated PKC at the membrane (~82%) resided in non-vinculin-containing regions of the cell surface, most likely the caveolar domain of the membrane. Experiments in non-permeabilized cells showed no specific immunolabeling with MAb 1.9 indicating that the PKC label in non-vinculin-containing areas did not represent a nonspecific caveolar uptake of the antibody. Beyond the 150-nm membrane annulus, and extending to 300 nm, the remaining 59.2% of the activated PKC-specific fluorescent signal was found to be primarily located in regions under the vinculin-rich areas located at the cell membrane. The subvinculin location of this pool of activated PKC was made readily apparent by projecting the distribution of this pool of activated PKC to the surface membrane below the vinculin in a radial direction to the depth of 300 nm. Analysis of these projection images indicated that ~80% of activated PKC located within 300 nm of the surface mapped to within ±150 nm of vinculin-containing voxels, a numerical confirmation of the

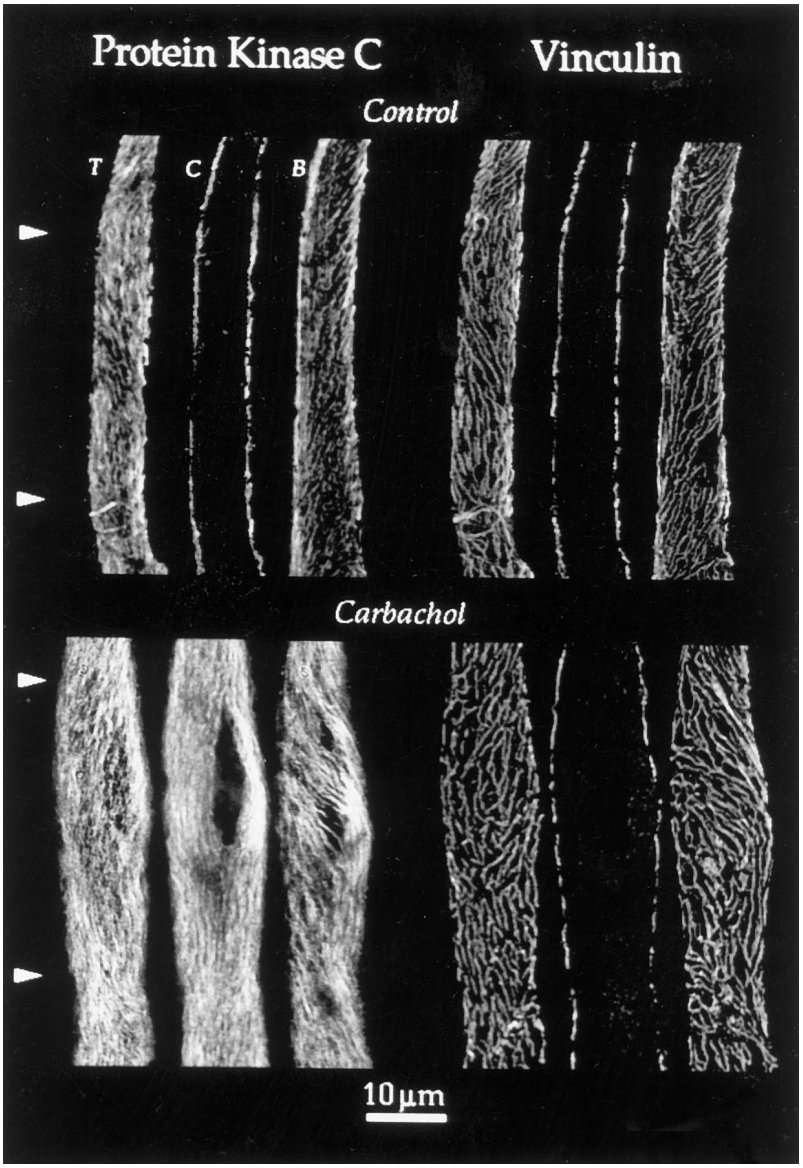

FIGURE 5 Immunofluorescent images of stomach smooth muscle cells dual-labeled for PKC (*left*) and vinculin (*right*). Cell images displayed at the top are for unstimulated resting cell; images displayed at the bottom are for a cell treated with carbachol (10 μM for 1 min). Images show the distribution of PKC and vinculin displayed as three 750-nm-thick sections in an *x-y* projection. Sections displayed represent the top (*T*), center (*C*), and bottom (*B*) views of the cell. Arrows at the left-hand cell margin indicate the location from which the cross-sectional views shown in Fig. 7 were obtained.

visual impression given by the stereo pairs (Fig. 8) is presented in Fig. 9. Compared to control cells, colocalization of membrane-localized activated PKC with vinculin was 12.3% (significantly lower than control, $p < 0.05$) after PMA, 22.0% after carbachol (not statistically different from control, $p < 0.05$), and was 15.0% after 4-α PMA (not statistically different from control, $p < 0.05$) (Table 1).

Analysis of activated PKC in cytosol

Numerical analysis of the distribution of activated PKC-specific fluorescence as a function of distance from the cell surface confirmed the change in activated PKC distribution (Fig. 9). In unstimulated control cells, activated PKC was most concentrated in an annular region 300 nm inside the vinculin-defined cell surface, as indicated by the peak fluorescent distribution. Treatment of cells with PMA or carbachol, but not 4-α PMA, significantly altered distribution of fluorescence such that the density of activated PKC-specific labeling further from the cell membrane had increased. Activated PKC labeling was distributed throughout the interior of the cell, no longer confined to a region close to the cell surface.

DISCUSSION

In resting smooth muscle cells, our data indicated that most activated PKC is located ~300 nm beneath the cell surface and is structurally organized into strands that are oriented roughly parallel to one another along the cell's long axis. This same pattern of organization was observed at the cell surface with vinculin. Ultrastructurally, smooth muscle has been shown to possess a uniquely organized membrane associated with electron-dense material reflecting zones of cell attachment (Gabella and Blondell, 1978). These bands were described as running along the cell's long axis and exhibiting branches and occasional interconnections. Elec-

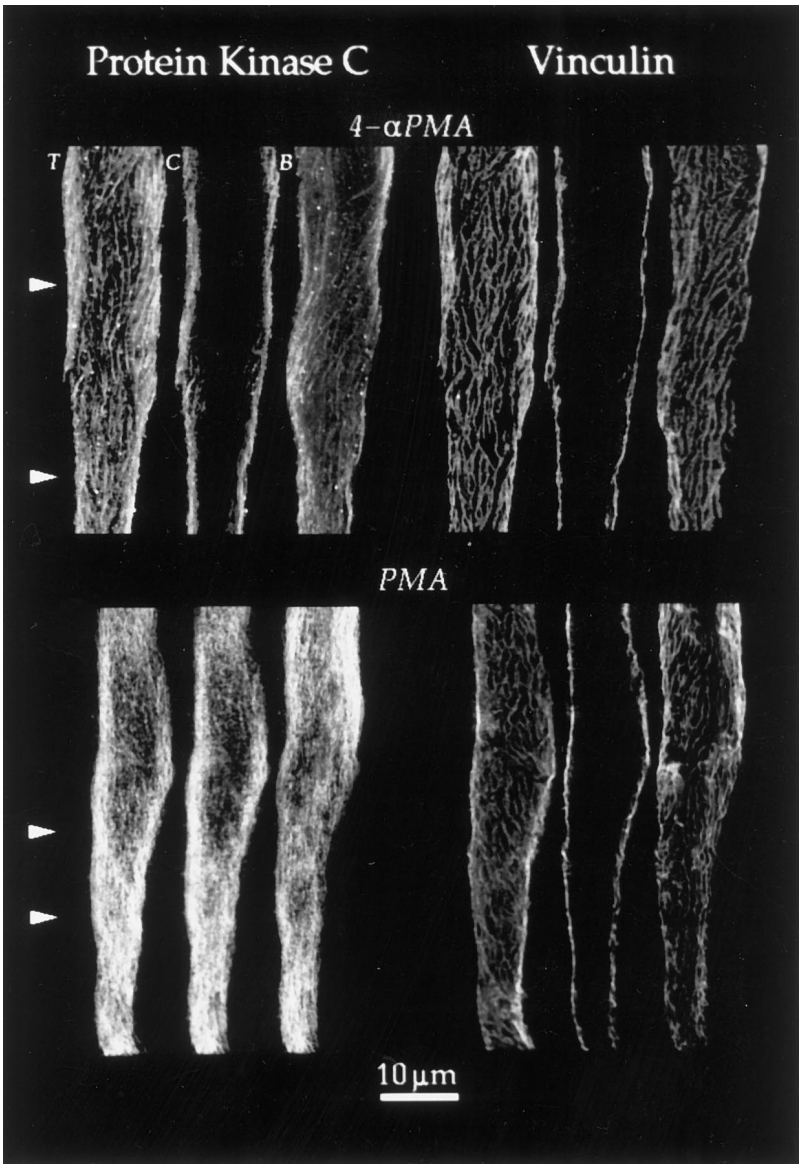

FIGURE 6 Distribution of PKC and vinculin in two single smooth muscle cells after one treatment with 4-α PMA (1 μM for 10 min) and PMA (1 μM for 10 min). Organization and conventions used in this figure are identical to those described for Fig. 5.

tron-dense bands were interspersed with bands of cell membrane containing caveolae. Thus, the membrane was defined as containing two structural domains, a cell attachment domain and a caveolar domain. In addition, interband spacing was ~0.35–0.40 μm, which is similar to the interband spacing of 0.5 μm that we observed. Collectively, these observations suggest that surface and subcellular molecular organization are related.

To examine whether activated PKC and vinculin were distributed in a coordinated manner, we analyzed the spatial relationship between fluorescent labels for activated PKC and vinculin. From this analysis we determined that in resting smooth muscle, ~41% of total activated PKC-specific signal was at the membrane (i.e., at or within 150 nm) and only 18% of this PKC was specifically colocalized with vinculin. Thus, most of the activated PKC at the membrane was distributed to non-vinculin-containing membrane regions such as the caveolar domain. The caveolar domain of the membrane is thought to play a central role in membrane Ca^{2+} handling (Rasmussen et al., 1987). It is potentially relevant that the sarcoplasmic reticulum often approaches to within 20 nm of individual caveolae (Gabella and Blondell, 1978). Moreover, previous work from this laboratory has established that within this functional domain of the membrane there is a close positional relationship between Na^+/K^+ ATPase and the Na^+/Ca^{2+} exchanger (Moore et al., 1993). Thus, the activated PKC near this region may be related to modulation of membrane ion exchange processes such as its postulated role in the regulation of Ca^{2+} handling by the plasma membrane and sarcoplasmic reticulum (Andrea and Walsh, 1992; Hug and Sarre, 1993; Nishizuka, 1984).

In the resting, unstimulated cells the presence, and restriction, of activated PKC near the membrane might be related to the existence of high calcium concentration near and under the membrane. In toad smooth muscle cells, measurement of near-membrane [Ca^{2+}] was accomplished

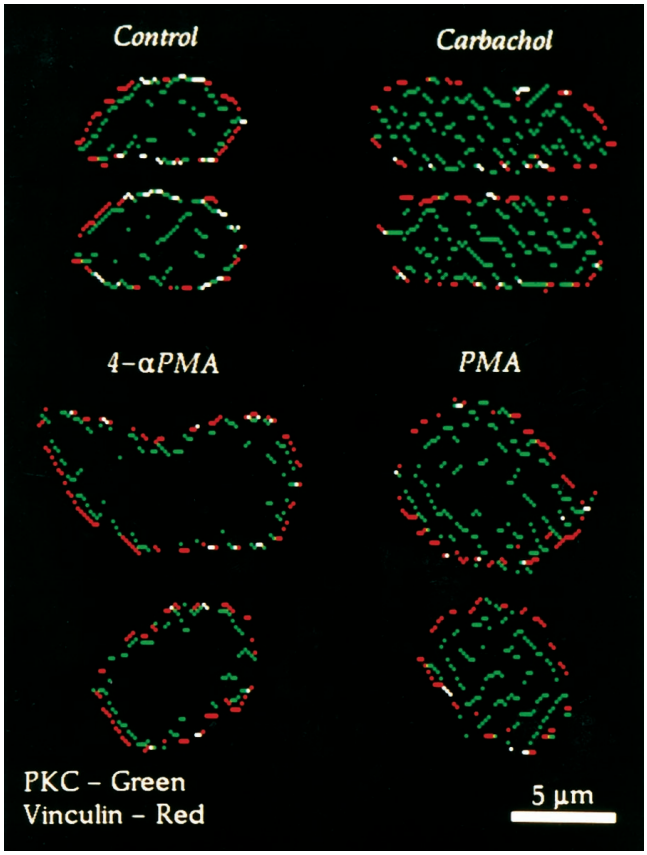

FIGURE 7 Relative distribution of PKC and vinculin in cross-sections of single smooth muscle cells in the presence or absence of agents expected to stimulate PKC activity. Cross-sectional segments of smooth muscle cells are shown for control and carbachol-treated cells displayed in Fig. 4 and for 4-α PMA (1 μM for 10 min) and PMA-treated (1 μM for 10 min) cells displayed in Fig. 5. These 150-nm-thick segments are a representation of the cells rotated by 90° in the *y* axis. Sections displayed were obtained from cells shown in Figs. 5 and 6 at the locations indicated by marginal arrows. In these sections, voxels have been pseudocolored to display PKC as green, vinculin as red, and superimposed voxels containing both PKC and vinculin as white. Black voxels contain neither.

using Ca^{2+} indicators that localize to the membrane or near-membrane space, such as FFP18 and C18-Fura-2 (Etter et al., 1994, 1996). Measurement of calcium with these dyes suggest that [Ca^{2+}] changes near the membrane are large and occur more rapidly than in the bulk cytoplasmic space. Similarly, in the rat aortic smooth muscle cell line A7r5, a membrane-targeting aequorin derivate, indicated that Ca^{2+} concentration in the cytoplasmic space beneath the plasma membrane increases to a greater degree after cell stimulation and is higher in unstimulated cells than in the bulk cytosol (Marsault et al., 1997). Thus, the presence of an elevated Ca^{2+} concentration in the near-membrane cytoplasmic space may, in part, explain the pool of activated PKC near the membrane.

A caveolar localization for membrane PKC has been reported by several different laboratories (e.g., Smart et al., 1995; Oku et al., 1997; Mineo et al., 1998). Our interpretation of a caveolar distribution for the membrane pool of activated PKC is consistent with these reports. The accumulation and targeting of active PKC in the caveolae appears to involve a docking mechanism associated with binding proteins located within the caveolae, such as caveolin (Oku et al., 1997; Mineo et al., 1998).

In unstimulated cells the remaining pool of activated PKC was ~59% of total activated PKC-specific signal and was located between 150 nm and 300 nm from the membrane. This pool of PKC exhibited a distribution pattern that was similar to the surface distribution pattern of vinculin, as indicated by the fact that the pattern of activated PKC distribution when projected to the surface mapped to regions containing vinculin to a high degree. This indicated that submembrane activated PKC was located beneath vinculin-rich regions in the plasma membrane. This suggested a close structural relationship between vinculin, PKC, and perhaps other proteins associated with the contractile filaments or their anchoring to the membrane (Schwartz, 1992; Turner and Burridge, 1991). A PKC labeling pattern resembling vinculin has also been described for rat embryo fibroblasts (Jaken et al., 1989). Vinculin is known to be but one protein among several involved in anchoring contractile filaments to integrins within the plasma membrane (Luna and Hitt, 1992; Turner and Burridge, 1991; Turner et al., 1989). Other proteins include vimentin, α-actinin, f-actin, paxillin, zyxin, tensin, and talin (Luna and Hitt, 1992; Turner and Burridge, 1991; Turner et al., 1989). A recent and potentially relevant study reported that Rack1, a receptor for activated PKC, binds to the β subunit of integrins (Liliental and Chung, 1998). This could provide an explanation for the accumulation of PKC in this region. In recent unpublished observations by D. Schmidt (personal communication), Rack1, PKC, and vinculin were all shown to exhibit similar overlapping distribution patterns in toad smooth muscle cells.

Our observations of PKC localization near vinculin are consistent with other studies that have shown that PKC mediated phosphorylation of proteins associated with the cell membrane anchorage complex. Phosphorylation of these proteins may be important in regulation of adhesion (Turner et al., 1989). Furthermore, the presence of activated PKC in the region of the contractile filaments may lead to phosphorylation of one or more of the proteins involved in contractile filament interaction and thus could be important in mediating Ca^{2+}-independent contractions in smooth muscle (Andrea and Walsh, 1992; Bradley and Morgan, 1987; Collins et al., 1992; Himpens et al., 1988; Moore et al., 1993; Hanks and Hunter, 1995; Rembold and Murphy, 1988; Stull et al., 1991). One difficulty with the concept that PKC is associated with contractile filament function was the early view that activated PKC is only localized to the plasma membrane. This view grew out of studies in which cell fractionation techniques have been used to separate PKC activity into a particulate (or membrane) pool and a cytosolic pool (Haller et al., 1990; Langlands and Diamond, 1992). In our study, after stimulation with either carbachol or phorbol esters, activated PKC was found to be located not only at the cell membrane, but also within the cell

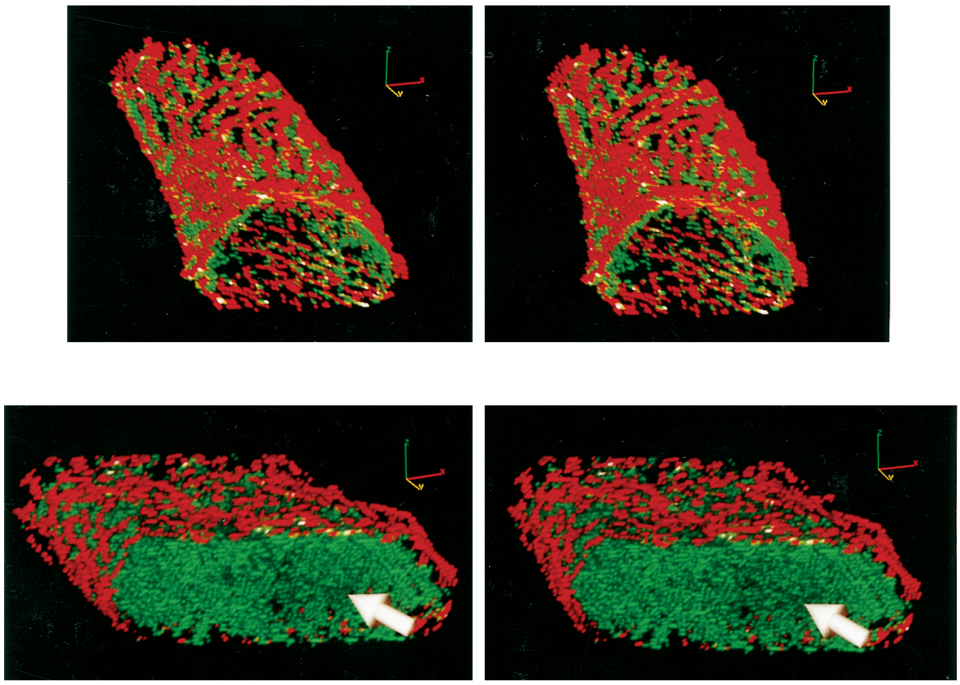

FIGURE 8 Stereo pairs of distribution of anti-PKC (MAb 1.9) and anti-vinculin staining in two smooth muscle cells, one stimulated with carbachol (1 μM for 1 min) (*bottom*) and the other untreated (*top*). The arrow in the carbachol images points to an open space devoid of PKC that contained the nucleus. Images are pseudocolored to display PKC-containing voxels as green, vinculin-containing voxels as red, and voxels containing both PKC and vinculin as white.

center. This cytosolic PKC was found to exhibit a filament-like distribution pattern in the smooth muscle cells. Thus, our observations provide support for the putative role of PKC in regulating membrane ion transport functions and contractile protein function.

While the view that upon activation PKC becomes associated with filamentous elements most likely involved in contraction appears to run contrary to views based on cell fractionation studies, other recent immunocytochemical studies have revealed somewhat similar results. Specifically in cardiac muscle and in cultured vascular smooth muscle (Haller et al., 1994; Liu et al., 1989; Mochly-Rosen et al., 1990), an increase in anti-PKC immunofluorescence associated with filaments has been observed after stimulation of PKC with either contractile agonists or phorbol esters. The specific PKC isozyme detected in the studies on cardiomyocytes was not well-defined, but was suggested to be the β isoform (Mochly-Rosen et al., 1990); in contrast, the isoform that appeared transiently on filaments in stimulated cultured vascular smooth muscle cell was the α isoform (Haller et al., 1994). The monoclonal antibody (MAb 1.9) used in our studies recognizes an epitope that may be present on more than one PKC isoform after activation. Thus, the results obtained in our study may reflect the distribution of more than one isoform. Further studies will be required with more specific problems to determine the distribution of individual PKC isoforms.

It is unlikely that all of the many isoforms of PKC that have been reported for smooth muscle (Ali et al., 1994; Andrea and Walsh, 1992; Assender et al., 1994; Donnelly et al., 1995; Haller et al., 1994; Khalil et al., 1992; Khalil and Morgan, 1992; Singer et al., 1992) are recognized by MAb 1.9 or are appearing on contractile filaments after stimulation. In general, the pattern of distribution of antibody

TABLE 1 Characteristics of activated PKC distribution in single smooth muscle cells

	Control	PMA	Carbachol	4-α PMA
Percent total signal at membrane				
Vinculin	89.0 ± 6.0 (5)	91.9 ± 3.0 (4)	89.5 ± 5.5 (4)	96.2 ± 1.80 (3)
Activated PKC	40.8 ± 7.6 (5)	24.5 ± 4.3 (4)	24.9 ± 3.5 (4)	36.8 ± 10.5 (3)
Colocalization of membrane-associated PKC and vinculin				
Vinculin with activated PKC	10.8 ± 4.1*	4.7 ± 3.5	10.6 ± 4.6*	8.4 ± 1.6*
Activated PKC with vinculin	17.9 ± 3.4*	12.3 ± 2.8#	22.0 ± 3.8*	15.0 ± 5.2*

The top of the table presents the fraction of total fluorescence intensity specific for vinculin and protein kinase C (PKC) that was located at the cell membrane; the bottom presents an analysis of the extent of colocalization of vinculin and activated PKC at the cell membrane. The first row presents the fraction of voxels containing vinculin that also contained activated PKC, while the second row presents the fraction of voxels containing activated PKC that also contained vinculin. Numbers in parentheses represent the number of cells analyzed.

*Observed overlap between the two proteins was less ($p < 95\%$) than would have been predicted if the two proteins were randomly distributed with respect to each other. Predicted overlap was generated from a random distribution whose variance was (Np) (1-p), where N was total number of voxels on the membrane, and p was the probability that a voxel contained both proteins.

#Significantly different from control.

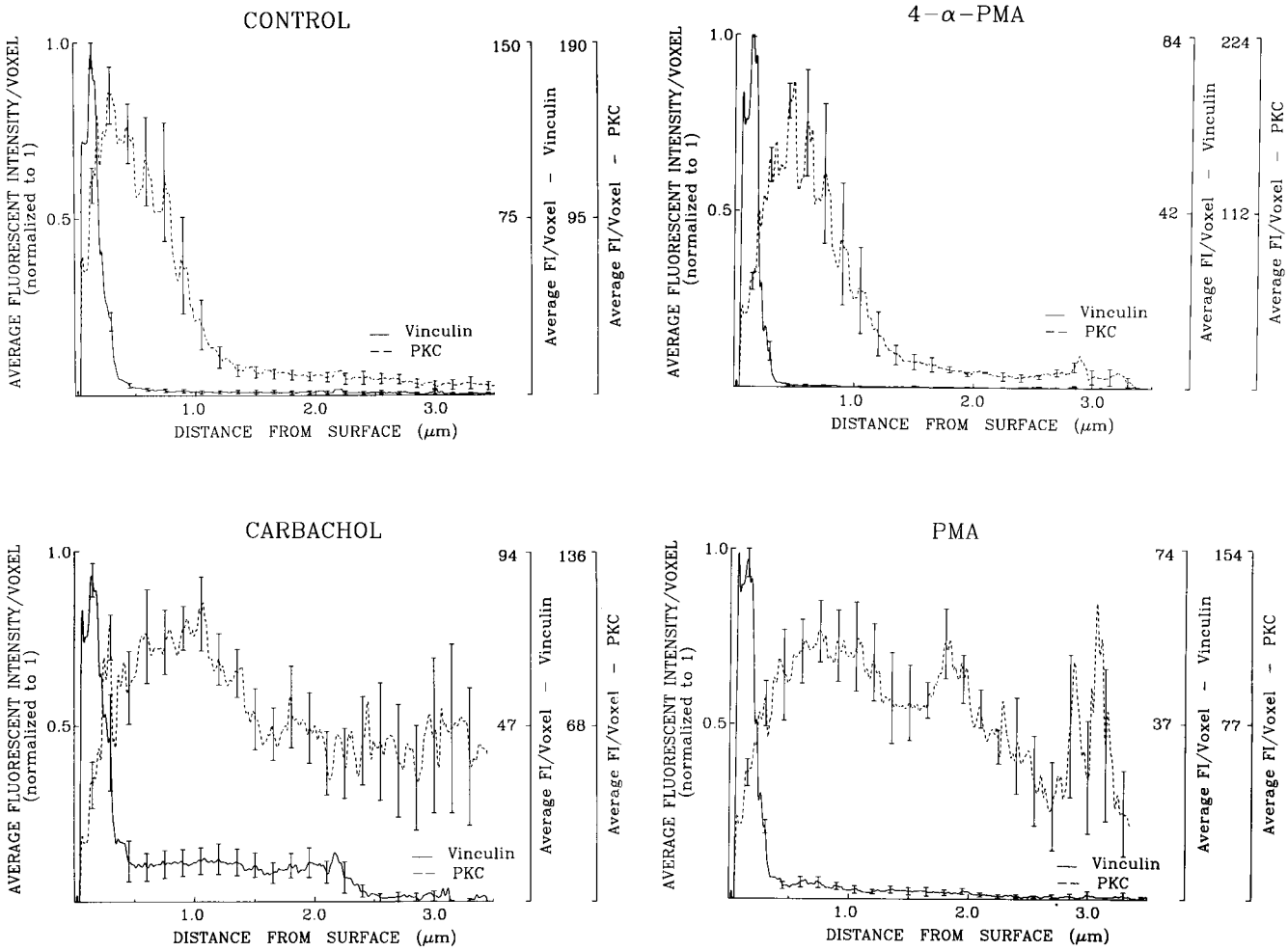

FIGURE 9 Radial distribution patterns of anti-PKC (MAb 1.9) and anti-vinculin staining density for control cells ($n = 5$) and cells treated with PMA (1 μM for 10 min) ($n = 4$), carbachol (10 μM for 1 min) ($n = 4$), or 4-α PMA (1 μM for 10 min) ($n = 3$). The histogram display shows average fluorescence intensity normalized for volume by expressing it as average fluorescent intensity per voxel as a function of distance from the cell surface for vinculin (*solid line*) and PKC (*dashed line*). The left *y* axis for PKC or vinculin was normalized to 1 with respect to vinculin, the right *y* axis shows the absolute values for the fluorescent intensities per voxel for each of the proteins.

staining for different PKC isoforms, both at rest and after stimulation, is quite isoform-specific in smooth muscle (Haller et al., 1994; Khalil et al., 1992; Khalil and Morgan; 1992) as well as in other cells (Hug and Sarre, 1993; Liu et al., 1989; Nishizuka, 1984). Ongoing work is therefore focused on determining which PKC isoform is being detected on the filaments after cell stimulation.

In our study, the increase in overall smooth muscle cell fluorescence after activation is interpreted as an increase in the total pool of activated PKC. This interpretation is consistent with findings of the immunoprecipitation experiments. Because the anti-PKC antibody used for immunolabeling prefers the active form of PKC, the change in distribution of activated PKC that we observed may not necessarily reflect a translocation event. Instead, activation of the kinase appears to improve access of the antibody to its PKC binding epitope. The presence of PKC within the cytosolic compartment after activation contrasts significantly with the view that activation involves strict translocation of activated PKC to the outer cell membrane (Asuoka et al., 1993; Nishizuka, 1984). The filament-like distribution of activated PKC within the cell center is consistent with functional studies showing that PKC could have access to and consequently have effects on the contractile mechanism.

We express our thanks to the following individuals for their assistance: Stephanie A. Hilliard for typing and proofing the manuscript, Katherine A. Kelly and Jon E. Mogford for assistance in performing immunoprecipitation experiments and Western blots, Dr. Arie Horowitz for performing cryosectioning, Jeff Collins for help with software development, and Drs. Walter A. Carrington and Dr. Ronald Lynch, and Kevin E. Fogarty for many helpful discussions about these data.

This study was supported by the following: National Institutes of Health Grants HL55050 and HL33324 and a CIBA-GEIGY Established Investigator Award (American Heart Association) (to G.A.M.); National Institutes of Health Grant HL14523 and National Science Foundation Grant BIR920007 (to F.S.F.); a grant-in-aid from the American Heart Association, Massachusetts affiliate and grants from the Medical Research Council of Canada and the Heart and Stroke Foundation of British Columbia and Yukon (to E.D.W.M.); and National Institutes of Health Grant DK09226 (to D.J.S.).

REFERENCES

Ali, S. M., W. Becker, M. G. Davis, and G. W. Dorn II. 1994. Dissociation of vasoconstrictor-stimulated fibroblast growth factor expression from hypertrophic growth in cultural vascular smooth muscle cells: relevant roles of protein kinase C. *Circ. Res.* 75:836–843.

Andrea, J. E., and M. P. Walsh. 1992. Protein kinase C of smooth muscle. *Hypertension*. 20:585–595.

Assender, J. W., E. Kontny, and B. B. Fredholm. 1994. Expression of protein kinase C isoforms in smooth muscle cells in various states of differentiation. *FEBS Lett.* 342:76–80.

Asuoka, Y., S. Hnakamura, K. Yoshida, and Y. Nishizuka. 1993. Protein kinase C, calcium, and phospholipid degradation. *TIBS*. 414–417.

Bradley, A. B., and K. G. Morgan. 1987. Alterations in cytoplasmic calcium sensitivity during porcine coronary artery contractions as detected by aequorin. *J. Physiol. (Lond.)*. 385:437–448.

Carrington, W. A. 1990. Image restoration in 3D microscopy with limited data. *SPIE Proc.* 1205:72–83.

Carrington, W. A., K. E. Fogarty, and F. S. Fay. 1990. 3D fluorescence imaging of single cells using image restoration. *Noninvasive Tech. in Cell Biol.* 53–72.

Collins, E. M., M. P. Walsh, and K. G. Morgan. 1992. Contraction of single vascular smooth muscle cells by phenylephrine at constant $[Ca^{2+}]_i$. *Am. J. Physiol.* 252:H754–H762.

Donnelly, R., K. Yang, M. B. Omary, S. Azhar, and J. L. Black. 1995. Expression of multiple isozymes of protein kinase C in airway smooth muscle. *Am. J. Respir. Cell Mol. Biol.* 13:253–256.

Etter, E. F., M. A. Kuhn, and F. S. Fay. 1994. Detection of changes in near-membrane Ca^{2+} concentration using a novel membrane-associated Ca^{2+} indicator. *J. Biol. Chem.* 269:10141–10149.

Etter, E. F., A. Mintu, M. Poenie, and F. S. Fay. 1996. Near-membrane $[Ca^{2+}]$ transients resolved using the Ca^{2+} indicator FFP18. *Proc. Natl. Acad. Sci. USA.* 93:5368–5373.

Fay, F. S., W. A. Carrington, and K. E. Fogarty. 1989. Three-dimensional molecular distribution in single cells analyzed using the digital imaging microscope. *J. Microsc.* 153:133–149.

Fay, F. S., R. Hoffman, S. Leclair, and P. Merriam. 1982. Preparation of individual smooth muscle cells from the stomach of *Bufo marinus*. *Methods Enzymol.* 85:284–292.

Gabella, G., and S. Blondell. 1978. Effect of stretch and contraction on caveolae of smooth muscle cells. *Cell Tissue Res.* 190:255–271.

Haller, H., P. Quass, C. Lindshau, F. C. Luft, and A. Distler. 1994. Platelet-derived growth factor and angiotensin II induce different spatial distribution of protein kinase C-alpha, beta in vascular smooth muscle cells. *Hypertension*. 23:848–852.

Haller, H., J. I. Smallwood, and H. Rasmussen. 1990. Protein kinase C translocation in intact vascular smooth muscle. *Biochem. J.* 270: 375–381.

Hanks, S. K., and T. Hunter. 1995. The eukaryotic protein kinase superfamily: kinase (catalytic) domain structure and classification. *FASEB J.* 9:576–596.

Himpens, B., G. Matthijs, A. V. Somlyo, T. M. Butler, and A. P. Somlyo. 1988. Cytoplasmic free calcium, myosin light chain phosphorylation, and force in phasic and tonic smooth muscle. *J. Gen. Physiol.* 92: 713–729.

Hug, H., and T. F. Sarre. 1993. Protein kinase C isoenzymes: divergence in signal transduction? *Biochem. J.* 291:329–343.

Jaken, S., K. Leach, and T. Klauck. 1989. Association of type 3 protein kinase C with focal contacts in rat embryo fibroblasts. *J. Cell Biol.* 109:697–704.

Khalil, R. A., C. Lajoie, M. S. Resnick, and K. G. Morgan. 1992. Ca^{2+} independent isoforms of protein kinase C differentially translocate in smooth muscle. *Am. J. Physiol.* 263:C714–C719.

Khalil, R. A., and K. G. Morgan. 1991. Imaging of protein kinase C distribution and translocation in living vascular smooth muscle cells. *Circ. Res.* 69:1626–1631.

Khalil, R. A., and K. G. Morgan. 1992. Phenylephrine-induced translocation of protein kinase C and shortening of two types of vascular cells of the ferret. *J. Physiol.* 455:585–599.

Langlands, J. M., and J. Diamond. 1992. Translocation of protein kinase C in bovine tracheal smooth muscle strips: the effect of metacholine and isoprenaline. *Eur. J. Pharmacol., Mol. Pharmacol. Sect.* 227:131–138.

Lifshitz, L. M. 1998. Determining data independence on a digitized membrane in three dimensions. *IEEE Trans. Med. Imaging*. 17:299–303.

Liliental, J., and D. D. Chang. 1998. Rack1, a receptor for activated protein kinase C, interacts with integrin beta subunit. *J. Biochem. Chem.* 273: 2379–2383.

Liu, J. D., J. G. Wood, R. L. Raynor, Y. C. Wang, T. A. Noland, A. A. Ansari, and J. F. Kuo. 1989. Subcellular distribution and immunocytochemical localization of protein kinase C in myocardium, and phosphorylation of troponin in isolated myocytes stimulated by isoproterenol or phorbol ester. *Biochem. Biophys. Res. Commun.* 162:1105–1110.

Luna, E. J., and A. L. Hitt. 1992. Cytoskeleton-plasma membrane interactions. *Science*. 258:955–964.

Marsault, R., M. Murgia, T. Pozzan, and R. Rizzota. 1997. Domains of high Ca^{2+} beneath the plasma membrane of living ATr5 cells. *EMBO J.* 16:1575–1581.

Mineo, C., Y. S. Ying, C. Chapline, S. Jaken, and R. G. W. Anderson. 1998. Targeting of protein kinase Cx to caveolae. *J. Cell Biol.* 141:601–610.

Mochly-Rosen, D. C. 1995. Localization of protein kinases by anchoring proteins: a theme in signal transduction. *Science*. 268:247–251.

Mochly-Rosen, D., C. J. Henrich, L. Cheever, H. Khaner, and P. C. Simpson. 1990. A protein kinase C isozyme is translocated to cytoskeletal elements on activation. *Cell. Reg.* 1:693–706.

Mochly-Rosen, D., and D. E. Koshland. 1987. Domain structure and phosphorylation of protein kinase C. *J. Biol. Chem.* 262:2291–2297.

Mochly-Rosen, D., and D. E. Koshland. 1988. A general procedure for screening inhibitory antibodies: application for identifying anti-protein kinase C antibodies. *Anal. Biochem.* 170:31–37.

Moore, E. D. W., E. F. Etter, K. D. Philipson, W. A. Carrington, K. E. Fogarty, L. M. Lifshitz, and F. S. Fay. 1993. Coupling of the Na^+/Ca^{2+} exchanger, Na^+/K^+ pump, and sarcoplasmic reticulum in smooth muscle. *Nature*. 265:657–660.

Morgan, J. P., and K. G. Morgan. 1984. Stimulus specific patterns of intracellular calcium levels in smooth muscle of ferret portal vein. *J. Physiol. (Lond.).* 351:155–167.

Nishizuka, Y. 1984. The role of protein kinase C in cell surface signal transduction and tumor promotion. *Nature*. 308:693–698.

Nishizuka, Y. T. 1992. Intracellular signaling by hydrolysis of phospholipid and activation of protein kinase C. *Science*. 258:607–614.

Oka, N., M. Yamamato, C. Schwencke, J. Kawabe, T. Ebina, S. Ohno, J. Covet, M. Lisanti, and Y. Ishikawa. 1997. Caveolin interaction with protein kinase C. *J. Biol. Chem.* 272:33416–33421.

Rasmussen, H., Y. Takuwa, and S. Park. 1987. Protein kinase C in the regulation of smooth muscle contraction. *FASEB J.* 1:177–185.

Rembold, C. M., and R. A. Murphy. 1988. Myoplasmic $[Ca^{2+}]$ determines myosin phosphorylation in agonist-stimulated swine arterial smooth muscle. *Circ. Res.* 63:593–603.

Schwartz, M. A. 1992. Transmembrane signaling by integrins. *Trends Cell Biol.* 2:304–308.

Singer, H. A., C. M. Schworer, C. Sweeley, and H. Benscoter. 1992. Activation of protein kinase C isozymes by contractile stimuli in arterial smooth muscle. *Arch. Biochem. Biophys.* 299:320–329.

Smart, E. J., Y. S. Ying, and R. G. Anderson. 1995. Hormonal regulation of caveolae internalization. *J. Cell Biol.* 131:929–938.

Stull, J. T., P. J. Gallagher, B. P. Herring, and K. E. Kamm. 1991. Vascular smooth muscle contractile elements: cellular regulation. *Hypertension*. 17:723–732.

Turner, C. E., and K. Burridge. 1991. Transmembrane molecular assemblies in cell-extracellular matrix interactions. *Curr. Opin. Cell Biol.* 3:849–853.

Turner, C. E., F. M. Pavalko, and K. Burridge. 1989. The role of phosphorylation and limited proteolytic cleavage of talin and vinculin in the disruption of focal adhesion integrity. *J. Biol. Chem.* 264:11935–11944.

Walsh, M. P., J. D. Carmichael, and G. J. Kargacin. 1993. Characterization and confocal imaging of calponin in gastrointestinal smooth muscle. *Am. J. Physiol.* 265:C1371–C1378.